Proceedings of the ASME/BATH
Symposium on Fluid Power and Motion Control
FPMC2019
October 7-9, 2019, Sarasota, Florida, USA

FPMC2019-1647

SWITCH-MODE POWER TRANSFORMER IN A WAVE-POWERED, REVERSE OSMOSIS DESALINATION PLANT

Jeremy W. Simmons II
Department of Mechanical Engineering
University of Minnesota
Minneapolis, MN, USA
simmo536@umn.edu

James D. Van de Ven
Department of Mechanical Engineering
University of Minnesota
Minneapolis, MN, USA
vandeven@umn.edu

ABSTRACT

In the reverse osmosis (RO) desalination process, a salt water solution is pressurized to overcome the osmotic pressure across a semi-permeable membrane. A few groups have proposed that a wave energy converter (WEC) having a seawater based, hydraulic power take-off can could be used to pressurize the feedwater for an RO system. However, coupling the wave energy harvesting process and the RO desalination process imposes unique design constraints on the fluid power system, such as pressure limits of conventional RO system components. In this study, a fluid power circuit with a switch-mode power transformer is used to transfer power while keeping the pressure of the power take-off and RO processes relatively decoupled. The switch-mode power transformer studied herein adds fewer costly components and less significant loss mechanisms to the system than a conventional hydraulic transformer performing the same function. The switch-mode power transformer uses the inertia of a hydraulic motor driven electric generator and switching of the hydraulic motor inlet between high and low-pressure sources to decrease the pressure at which power is being transmitted to the RO process. This process is analogous to DC-DC switching power transformers in the electrical domain. This study seeks to demonstrate this unique switch-mode system as a potential solution for coupling the wave-energy harvesting process with the reverse osmosis process. The system is modeled and studied in the context that the transformer and RO system are onshore, 500 meters from the WEC. Power captured from the WEC is transmitted through a long pipeline to shore. A distributed parameter model is used to model the pipeline dynamics, simultaneously revealing the significance of these dynamics and the robustness with which the switch-mode transformer decouples the pressure dynamics at the RO feed from the pipeline dynamics. The switch-mode power transformer is estimated to be 76% efficient while the system, as a whole, is estimated to be 45% efficient.

INTRODUCTION

For many coastal locations, ocean wave energy is a substantial resource but is challenging to covert directly to electricity. However, hydraulic power-take-offs (PTOs) are well suited for the low speeds and high forces that are characteristic of wave energy converter (WEC) operation as well as the high-speed, low torque that is more suitable for electrical power generation, allowing easier coupling of the energy harvesting and electrical power generation. There have been a few WECs demonstrated having hydraulic PTOs [4] [5] and several computer-aided design studies exploring their use [3]–[6]. There has also been a recent effort in the design and testing of a universal WEC PTO using a fluid power circuit named WavePOD [7].

Beyond generating electricity, several groups have considered harvesting the energy of ocean waves as an alternative to using diesel generators and photovoltaic devices to power seawater desalination plants, specifically reverse osmosis (RO) desalination [8]–[10]. In fact, a number of groups have explored the direct coupling of the PTO and RO fluid power circuits [9], [11], [12].

In the RO desalination process, filtered seawater is pressurized to overcome the osmotic pressure across a semi-permeable membrane. A fraction of the water permeates across the membrane while high salt concentration brine is discharge through a separate port.

Of course, significant challenges arise in designing a coupled system to be reliable. In addition to the challenges of all wave energy systems, the added challenges are that 1) the fluid power components must work with seawater as the working fluid, 2) the feed pressure of the RO system is limited to about 700 – 1200

psi, and 3) the feed water pressures dynamics must be smooth so that the relatively fragile RO system components (e.g. RO membrane elements) are not damaged.

The schematic in Figure 1 illustrates a baseline hydraulic WEC PTO that generates both electricity and potable water. This system includes 1) a WEC-driven actuator and check valve rectifier that together function as a pump, 2) an RO system comprised of the RO membrane module and an optional energy recovery unit (ERU) to recover power from the high-pressure brine that would otherwise be throttled, 3) a charge pump that resupplies seawater consumed in the RO process, and 4) an electric generator driven by a hydraulic motor that supplies the electrical power demands of the plant. For serviceability, the RO system and genset are installed onshore while the WEC is offshore. The seawater is pumped through the long pipelines connecting these parts of the plant, which are separated by a distance on the order of 500 meters. High-pressure accumulators (HPAs) and a low-pressure accumulator (LPA) are implemented for smoothing the highly variable power associated with the oscillatory WEC motion. Without the RO system, this system is similar to the general approach taken for the WavePOD [7].

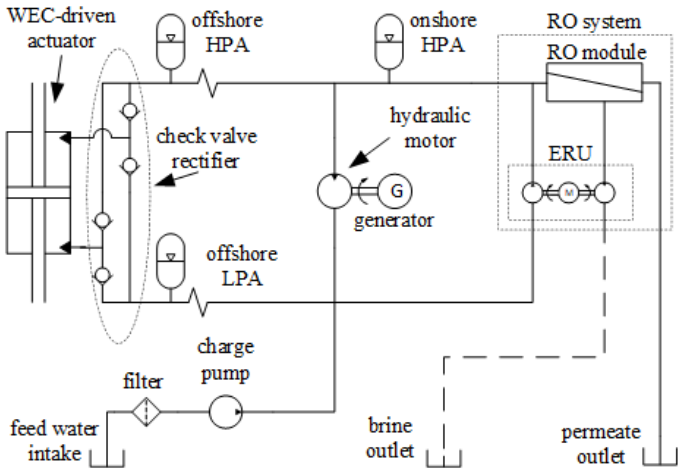

FIGURE 1. SIMPLE WAVE-POWERED RO DESALINATION PLANT WITH ELECTICAL POWER GENERATION.

This baseline system design has three inherent drawbacks stemming from the pressures of the WEC-driven actuator and the RO system being closely coupled. First, is that the range of pressures required for an RO system (about 700 – 1200 psi) are lower than typical hydraulic systems. The low operating pressures require higher flow rates and larger components than would be if the PTO were operated at higher pressures. Second, load control on the WEC is limited by the RO operation. Thirdly, the plant must be designed to keep the magnitude of pressure variations in the onshore HPA low to avoid damage to the RO system; this would require very large accumulators.

As an alternative, the pressures at which the PTO and RO system each operate could be decoupled with a hydraulic transformer. The circuit shown in Figure 2 implements a variable displacement motor and fixed displacement pump to form a conventional hydraulic transformer. This approach allows downsizing the WEC-driven actuator and pipelines to shore, as they can operate at a higher pressure, and allows more flexible control of the load on the WEC. However, this adds costly components and significant sources of power loss.

A switch-mode power transformer is proposed in this work in the place of the conventional transformer. This transformer, which is illustrated in Figure 3, uses the same components as the baseline system in Figure 1 and adds only two valves: a two-way switching valve and a check valve. This circuit allows the same pressure transformation as the conventional hydraulic transformer through pulse-width-modulated (PWM) control, or some other type of switching control, of the two-way valve.

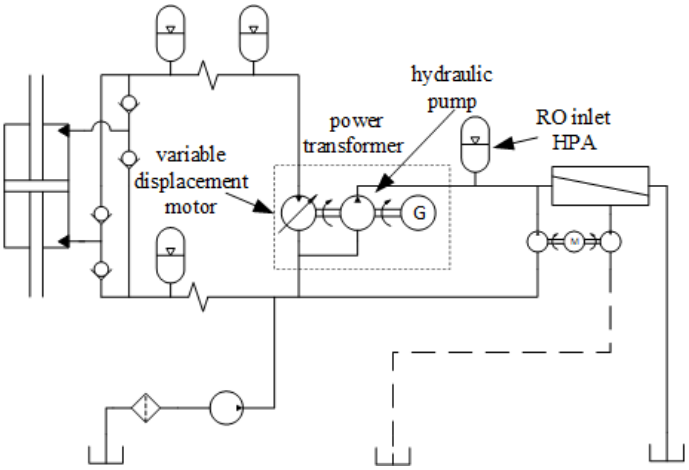

FIGURE 2. WAVE-POWERED RO DESALINATION PLANT WITH A CONVENTIONAL POWER TRANSFORMER.

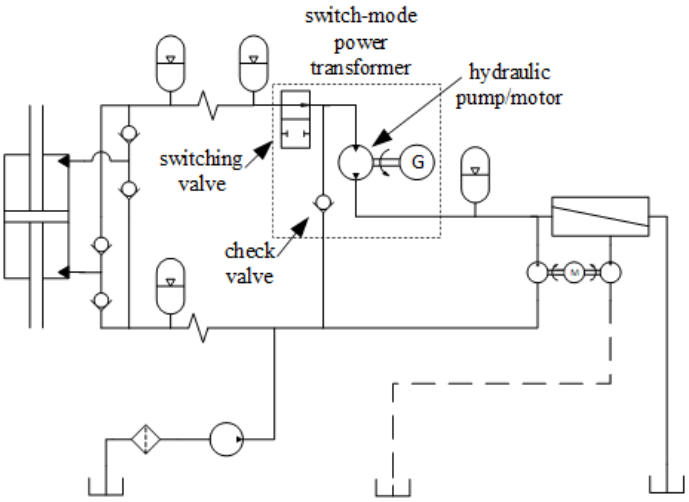

FIGURE 3. WAVE-POWERED RO DESALINATION PLANT WITH A SWITCH-MODE POWER TRANSFORMER.

The Switch-Mode Power Transformer

The proposed switch-mode power transformer is analogous to the switch-mode power supplies in the electronic domain. These use an inductor switched between high and low voltages, storing energy in and releasing energy from a magnetic field. Several analogous hydraulic circuits have been explored. Some have used the inertia of the working fluid in a long pipe to store energy [13] while others have used the inertia of a pump/motor and flywheel [14]. The power transformer considered herein uses the inertia of the hydraulic pump/motor and generator as the system inductance.

The switch-mode power transformer operates through the fast switching of the two-way valve between discrete states. In these discrete states, the pump/motor operates in either a pumping mode or a motoring mode. When the valve is open, the inlet to the pump/motor is connected to the high-pressure accumulator upstream and operates as a motor. In this mode, the pump/motor accelerates the generator rotor, storing kinetic energy. When the valve is closed, the inlet to the pump/motor is connected to the low-pressure outlet of the charge pump and operates as a pump. In the pump mode, the pump/motor uses energy stored in the generator rotor to drive the working fluid. The mean flow rate supplied to the RO system is maintained by converting excess mechanical power to electricity.

The power transformation is modulated by the length of time spent in either discrete state during each pulse cycle. This is described by the duty ratio, D, given by

$$D = \frac{t_h}{T_{sw}} \tag{1}$$

where T_{sw} is the switching period and t_h is the length of time the switching valve is open. The switching period is the inverse of the switching frequency, f_{sw}.

This study seeks to demonstrate this unique switch-mode system as a potential solution for coupling the wave-energy harvesting process with the RO process by illustrating the behavior of the plant and quantifying the performance of a preliminary design. A mathematical model, presented in the next section, is solved numerically to demonstrate and quantify the performance. Prescribed, sinusoidal displacements are used to simulate the WEC motion driven by regular waves. The following section presents the mathematical models used to model this plant design. The next describes details of the design; specifically, the control laws used to regulate the plant are described and the parameters used in the simulation of the model are given. The section that follows presents simulation results along with the mean power losses, subsystem efficiencies, and a discussion. The final section concludes the paper.

MODELING

The model used in this study includes the entire fluid power circuit shown in Figure 3, except the RO system. The input to the system model is the motion of the WEC-driven actuator. The outputs are the surplus electrical power generated and the seawater supplied to the RO system.

The system has been re-represented for modeling in Figure 4. Pressure nodes are labeled with the variable name used in modeling (p is used generically). The compressible volumes of fluid are indicated by a fluid volume and their variable name (V is used generically). The flow rates modeled and their variable names (q is used generically) are indicated by arrows pointing across their path and in the direction of positive flow. The position of the WEC-driven actuator, x, has the zero-position centered about the limits of travel.

The RO system is represented as two flow sinks, with the high-pressure feed flow rate, q_{RO}, equal to the permeate flow rate, q_{perm}, and the low-pressure flow rate, $q_{ERU,in}$, equal to the discharged brine flow rate, q_{brine}. This assumes the ERU, as shown in Figure 1, is comprised of a pump and motor having equal displacement.

The position of the WEC-driven actuator is prescribed in this study. Specifically, the position of the WEC-driven actuator is assumed to be sinusoidal such that

$$x = |x| \sin\left(2\pi \frac{t}{T_w}\right) \tag{2}$$

where T_w is the wave period. In the case of a near constant reaction force of the PTO, the mean power captured by the WEC can be characterized by its mean absolute velocity, $|\dot{x}|_{ave}$. Thus, the magnitude $|x|$ can be determined such that

$$|x| = |\dot{x}|_{ave} \frac{T_w}{4} \tag{3}$$

The mathematical models of the components and the components' power losses follow.

WEC-Driven Actuator

Two fluid volumes are created by the two chambers of the WEC-driven actuator and the intermediate piping between the actuator and the check valve rectifier. The pressure dynamics in these volumes are modeled using the definition of the bulk modulus such that

$$\frac{dp}{dt} = \frac{\beta_{eff}}{V}\left(\frac{dV}{dt} - q_{out}\right) \tag{4}$$

where β_{eff} is the effective bulk modules of the fluid, V is the instantaneous volume and q_{out} is the net flow rate out of the volume.

The effective bulk modulus of the fluid is typically pressure dependent due to the entrainment of air. The model proposed by

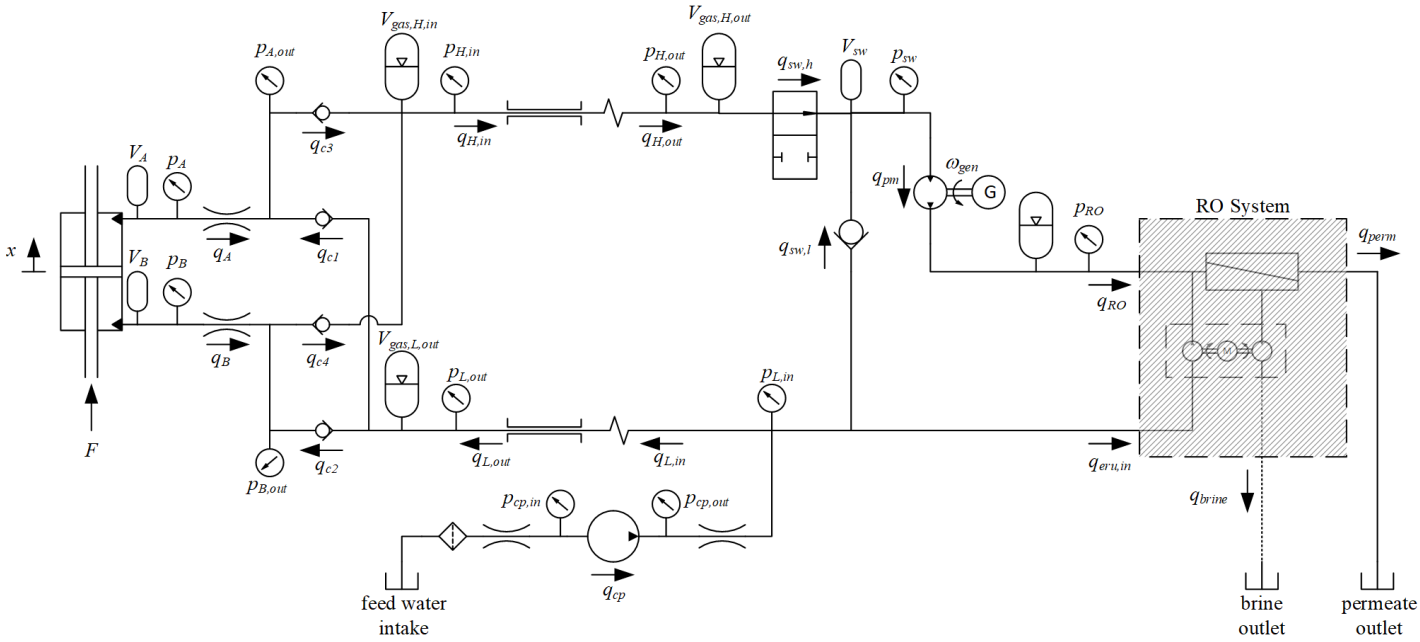

FIGURE 4. MODELING SCHEMATIC OF THE WAVE-POWERED RO PLANT.

Cho at al. is used, which considers the bulk modulus of a pure fluid and the compliance of an isentropically compressed volume fraction of air [15]:

$$\beta_{eff}(p) = \beta\left(\frac{\left(\frac{p}{p_o}\right)^{\frac{1}{\gamma}} e^{\frac{(p_o-p)}{\beta}} + R}{\frac{R}{\gamma}\frac{\beta}{p} + \left(\frac{p}{p_o}\right)^{\frac{1}{\gamma}} e^{\frac{(p_o-p)}{\beta}}}\right) \tag{5}$$

where β is the bulk modulus of the pure liquid, γ is the heat ratio of air, and R is the entrained air volume fraction at some absolute pressure p_o,

The instantaneous volume of each fluid volume depends on the actuator position. These volumes are described by

$$V_A = A_{piston}\left(\frac{L_{stroke}}{2} - x\right) + V_{int} \tag{6}$$

and

$$V_B = A_{piston}\left(\frac{L_{stroke}}{2} + x\right) + V_{int} \tag{7}$$

where A_{piston} is the area of the actuator piston, L_{stroke} is the length of the actuator's stroke, and V_{int} is the volume of the line intermediate to the check valve rectifier.

The force driving the actuator, F, is calculated from an assumed, constant mechanical efficiency. However, because the fluid volume in the actuator can store energy, this energy can cause work to be done on the WEC by the compressed volume and thereby the WEC can do work on its surroundings. Therefore, the force between the WEC and the actuator is formulated as

$$F = \begin{cases} \eta_{WEC}(p_A - p_B)A_{piston} & if\ \dot{x}(p_A - p_B) < 0 \\ \dfrac{(p_A - p_B)A_{piston}}{\eta_{WEC}} & if\ \dot{x}(p_A - p_B) \geq 0 \end{cases} \tag{8}$$

where η_{WEC} is the mechanical efficiency of the WEC-driven actuator.

Intermediate Line

It is assumed that some intermediate piping exists between the WEC-driven actuator and the check valve rectifier. The pressure-drop across this piping is modeled by the Darcy-Weisbach equation formulated for pressure and flow rate.

$$\Delta p(q) = f\frac{\rho l q^2}{2dA^2} \tag{9}$$

where f is the Darcy friction factor, l is the length of the pipe, d is the inner diameter of the pipe, and A is the flow area of the pipe. The Blasius correlation is used to estimate the Darcy friction factor in the turbulent regime (Re > 4500) and an interpolation is used between the laminar and turbulent regimes (2300 < Re < 4500). This gives the following piecewise function:

$$f = \begin{cases} \dfrac{64}{Re} & if\ Re \leq 2300 \\ f(2300) + \dfrac{f(4500) - f(2300)}{2200}(Re - 2300) & if\ 2300 < Re < 4500 \\ 0.316Re^{-\frac{1}{4}} & if\ Re \geq 4500 \end{cases} \tag{10}.$$

Accumulators

The variations in pressure in the accumulators relevant to this study are assumed to be fast with respect to the any dissipation of heat. The plant is also assumed to operate near room temperature. Therefore, the compression of the charged gas is modeled as isentropic compression of an ideal gas. This gives the pressure of the accumulator as

$$p(V_{gas}) = p_{charge}\left(\frac{V_{charge}}{V_{gas}}\right)^{\gamma} \tag{11}$$

where V_{gas} is the volume of the charged gas, p_{charge} is the pressure that the accumulator is initially charged to, and V_{charge} is the initial charged volume. The dynamics of the volume of gas are such that

$$\frac{dV_{gas}}{dt} = (q_{out} - q_{in}) \tag{12}$$

where q_{in} and q_{out} are the flow into and out of the pressure node, respectively, and depend on the accumulator.

The stiffness and inertia of the diaphragm, as well as the resistance to fluid flow in and out of the accumulators are not considered. Therefore, having also assumed the compression of gas to be isentropic, hysteretic effects are neglected.

Valves

The flow rates through the check valves and the two-way switching valve are modeled by the orifice equation:

$$q(\Delta p, A) = C_d A \frac{\Delta p}{|\Delta p|}\sqrt{\frac{2}{\rho}|\Delta p|} \tag{13}$$

where C_d is the discharge coefficient, A is the instantaneous flow area, and Δp is the pressure drop in the positive flow direction, generically.

Check Valves The flow areas of the check valves are modeled by the following piecewise function:

$$A = \begin{cases} 0 & if\ \Delta p < p_{crack} \\ A_{max}\dfrac{\Delta p - p_{crack}}{2p_{crack}} & if\ p_{crack} < \Delta p < 3p_{crack} \\ A_{max} & if\ \Delta p > 3p_{crack} \end{cases} \tag{14}$$

where p_{crack} is the pressure difference at which the valve begins to open and A_{max} is the maximum flow area. The transition of the valve area for pressure differences between the cracking pressure and three times the cracking pressure is implemented for purely practical reasons to mitigate numerical oscillations.

Switching Valve The instantaneous flow area of the switching valve is modeled as a trapezoidal profile in time with a specified transition time. The ratio of time spent open with respect to the switching period is the duty ratio, as given in Eq. (1).

Long Line Model

The long pipeline between the WEC and shore is model using a distributed parameter system with unsteady friction. This adds significant computational expense over a lumped parameter model. However, lumped parameter models are typically only appropriate for line lengths that are less than 4% of the wavelength of a significant excitation. The wavelength of a cyclic excitation, λ_{ex}, is the distance a pressure wave travels before the next excitation and can be estimated using the frequency of the excitation, f_{ex}, and an approximation of the speed of sound, a, by

$$\lambda_{ex} = \frac{a}{f_{ex}} \tag{15}.$$

The system explored in this work has two separate excitations: the oscillatory flow from the WEC-driven actuator and the switching of the switch-mode power transformer. The excitation from the switching might be negligible if the switching frequency is high and the onshore accumulator upstream of the transformer has a very large volume (therefore causing a negligible flow ripple). However, the oscillatory flow of the WEC-driven actuator is not negligible. Typical wave periods are in the range of 6-12 seconds. With flow rectification, the frequency of excitation is 0.17-0.33 Hz generating a wavelength that is on the order of the pipeline length.

In this work, the Method of Characteristics (MOC) is used to solve the momentum and continuity equations. This is an efficient time-domain method for modeling line dynamics as it reduces the partial differential momentum and continuity equations for compressible fluid flow to two ordinary differential equations [16]. This requires that the equations are solved along the characteristics for the system of PDEs given by

$$\pm a = \frac{\Delta x}{\Delta t} \tag{16}.$$

where a is the sonic velocity, Δx is the spatial step size and Δt is the time step size. Note that this definition of the characteristics assumes a negligible flow velocity with respect to the sonic velocity. Assuming a thick-walled pipe, the sonic velocity is

$$a_{eff} = \sqrt{\frac{\beta_{eff}(p)}{\rho}} \tag{17}.$$

An increase in piping loss occurs in unsteady flow due to in-plane velocity waves. Trikka formulated an approximation of the analytical solution for the unsteady friction loss [17]. This

formulation, with the weighting coefficients given by Schohl [18], is used to model the unsteady friction in this work. Yudell provides detail on the implementation of this pipeline model [19].

Pump/Motor and Generator

The pump/motor is modeled by definitions of mechanical and volumetric efficiency. However, the pump/motor switches between pumping and motoring modes with the switching of its inlet between high and low pressures. This necessitates piecewise definitions of these efficiencies, which follow.

The brake torque generated by the pump/motor is modeled as

$$T_{pm} = \begin{cases} \dfrac{D_{pm}\,(p_{sw} - p_{RO})}{\eta_{m,pm}} & if\ p_{sw} < p_{RO} \\ \eta_{m,pm} D_{pm}\,(p_{sw} - p_{RO}) & if\ p_{sw} > p_{RO} \end{cases} \quad (18)$$

where $\eta_{m,pm}$ is the mechanical efficiency and D_{pm} is the kinematic displacement per radian.

The flow rate passed through the pump motor is modeled by

$$q_{pm} = \begin{cases} \eta_{v,pm} D_{pm} \omega & if\ p_{sw} < p_{RO} \\ \dfrac{D_{pm}\omega}{\eta_{v,pm}} & if\ p_{sw} > p_{RO} \end{cases} \quad (19)$$

where $\eta_{v,pm}$ is the volumetric efficiency, and ω is the angular velocity in radian per second. The pump/motor power loss is given by

$$P_{pm,loss} = q_{pm}\,(p_{sw} - p_{RO}) - T_{pm}\omega \quad (20).$$

The generator might also switch modes between motor and generator operation if proper hardware was implemented so that the pump/motor could be driven independent of power delivered offshore. However, this study does not consider this mode of operation. The electrical power generated is modeled assuming a constant efficiency such that

$$P_{gen,elec} = \eta_{gen} T_{gen} \omega \quad (21)$$

where η_{gen} is the efficiency of the generator and T_{gen} is the brake torque and is defined as positive in the direction of ω. In this study, the torque is assumed to be directly controllable. The power loss of the generator is

$$P_{gen,loss} = T_{gen}\omega - P_{gen,elec} \quad (22).$$

The dynamics of the shaft angular velocity are modeled by

$$\frac{d\omega}{dt} = \frac{1}{I_{gen}}\left(T_{pm} - T_{gen}\right) \quad (23).$$

where I_{gen} is the moment of inertia of the generator rotor and the rotating components of the pump/motor. Bearing friction has been neglected in favor of modeling the mechanical efficiency.

Charge Pump

The charge pump is assumed to maintain the onshore low-pressure node at a constant pressure; that is, $p_{L,in}$ is modeled as constant. Therefore, the flow rate through the charge pump is

$$q_{cp} = q_{L,in} + q_{sw,l} + q_{ERU,in} \quad (24).$$

The electrical power consumed by the charge pump is

$$P_{cp,elec} = \frac{q_{cp}\left(p_{cp,out} - p_{cp,in}\right)}{\eta_{cp}\eta_{motor}} \quad (25)$$

where η_{cp} is the pump efficiency, η_{motor} is the efficiency of the electric motor driving the pump. These efficiencies have been assumed constant. The power loss for the charge pump is

$$P_{cp,loss} = P_{cp,elec} - q_{cp}\left(p_{cp,out} - p_{cp,in}\right) \quad (26).$$

Seawater Intake

The intake lines are model as a lumped pipe resistance. As with the intermediate lines, the pressure drop is given by Eq. (9) such that

$$p_{cp,in} = p_o - \Delta p\left(q_{cp}\right) \quad (27)$$

and

$$p_{cp,out} = p_{L,in} + \Delta p\left(q_{cp}\right) \quad (28)$$

where p_o is atmospheric pressure (101.3 kPa). The resistive power loss in the intake line is given by

$$P_{intake,loss} = q_{cp}\left(p_o - p_{cp,in} + p_{cp,out} - p_{L,in}\right) \quad (29)$$

DESIGN

This section presents aspects of design relevant to this initial study of this system. First, the control system used to regulate the plant is presented. Then, the system and component sizing is presented along with the parameters used in the numerical simulation of the system.

Control

Two separate controllers are used to regulate the plant. The states requiring control are the RO feed pressure, p_{RO}, and the pressure of the onshore HPA, $p_{H,out}$. The pressure in the onshore HPA upstream of the power transformer sets the pressure

differential, or load, on the WEC. Two control inputs are assumed to be available: the torque of the generator and the duty ratio of the switching valve.

RO Feed Pressure Control of RO feed pressure is accomplished using the torque of the generator as the control input.

In steady-state, the flow through the pump/motor would ideally match the high-pressure flow passed to the RO system, q_{RO}. However, the brake torque of the pump/motor switches between two extremes with the switching of the inlet pressure source. To fix the speed of the pump/motor the torque demand from the generator must mirror that of the pump/motor. However, this variation in generator torque may not be reasonable or desirable for the electrical system.

To reduce the variation in the torque demanded of the generator, and instead allow the speed of the pump/motor to vary about the mean steady-state speed, we introduce a first order low-pass filtered signal of p_{RO} as the controlled system output, $p_{RO,lpf}$, such that

$$\frac{dp_{RO,lpf}}{dt} = \frac{1}{\tau}\left(p_{RO} - p_{RO,lpf}\right) \quad (30).$$

where τ is the time constant of the filter. For a sufficiently low filter time constant, the control-loop remains stable. However, the time constant should be large enough so that cut-off frequency is lower than the switching frequency of the power transformer and the generator torque ripple is effectively reduced.

Proportional-integral-derivative (PID) control is used. The control law is

$$T_{gen} = k_{p,1}e_1 + \int k_{i,1}e_1 dt + k_{d,1}\frac{de_1}{dt} \quad (31)$$

where $k_{p,1}$, $k_{i,1}$, and $k_{d,1}$ are control gains and e_1 is the error between the reference feed pressure, $p_{RO,ref}$, and $p_{RO,lpf}$. The definition of error used is

$$e_1 = p_{RO,ref} - p_{RO,lpf} \quad (32).$$

WEC Load Control The duty of the switching valve is used as the control input to control $p_{H,out}$. Note that the duty must be bound between zero and unity. Proportional-integral (PI) control with a feedforward term is used such that

$$D = \min\left(1, \max\left(0, D_{ff} - k_{p,2}e_2 - \int k_{i,2}e_2 dt\right)\right) \quad (33)$$

where D_{ff} is the feedforward term and e_2 is the error between the pressure setpoint, $p_{H,out,ref}$, and $p_{H,out}$. The following definition of error is used:

$$e_2 = p_{H,out,ref} - p_{H,out} \quad (34).$$

Gains The controller gains used in this study are given in Table 1.

TABLE 1. CONTROLLER GAINS

RO feed pressure control	
Filter time constant, τ	0.1592
$k_{p,1}$	$3\text{x}10^{-3}$
$k_{i,1}$	$9\text{x}10^{-3}$
$k_{d,1}$	$1\text{x}10^{-3}$
Load control	
$k_{p,2}$	$1\text{x}10^{-8}$
$k_{i,2}$	$1\text{x}10^{-7}$

Sizing/Plant Operation

The system in this work is sized to produce 1000 cubic meters per day of potable water. The target mean input power to the WEC is 200 kW. Such a plant could be driven by a single WEC, such as the Oyster 1 which was rated for 315 kW [2], or a number of WECs in parallel having lower power ratings, such as the SurgeWEC developed by Resolute Marine Energy [8]. The nominal pressure differential across the input actuator is taken to be 30 MPa. Reverse osmosis systems using spiral-wound membrane elements are typically rated for either 1000 or 1200 psi. We assume a system operating with a target 1000 psi feed pressure.

Rühlicke and Hagg discuss practical design challenges for the actuators used for the Oyster 1 and suggest that these were designed for a mean absolute velocity of 0.16 m s^{-1} [20]. This value is used for $|\dot{x}|_{ave}$ in the calculation of the WEC-driven actuator position. The mean WEC input power and nominal pressure differential of the actuator fix the desired mean flow rate driven by the actuator. Therefore, this mean absolute velocity establishes a required displacement of the actuator. The parameters for the WEC-driven actuator are provided in Table 2.

The check valves that comprise the check valve rectifier are sized to give a pressure drop of 3 bar at peak flow. Likewise, the switching valve and check valve leading to the pump/motor are sized to give a pressure drop of 3 bar at a flow rate equal to the mean pump/motor flow rate. The parameters for these valves are given in Table 3.

The remaining model parameters used in this study have been tabularized below. The physical properties of the working fluid and the accumulator charge gas are given in Table 4. The parameters for the pipelines are given in

Table 5, accumulators in Table 6, and the switch-mode transformer in Table 7. The assumed component efficiencies are given in Table 8.

TABLE 2. WEC PUMP PARAMETERS

Actuator piston area, A_{piston}	0.04	m^2
Actuator stroke, L_{stroke}	1.2	m

TABLE 3. VALVE PARAMETERS

Discharge coefficient, C_d	0.6	
High-pressure rectifier check valves		
Maximum flow area, A_{max}	0.0007	m^3
Cracking pressure, p_{crack}	100	kPa
Low-pressure rectifier check valves		
Maximum flow area, A_{max}	0.0007	m^3
Cracking pressure, p_{crack}	100	kPa
Switch-mode transformer check valve		
Maximum flow area, A_{max}	0.0012	m^3
Cracking pressure, p_{crack}	100	kPa
Switch-mode transformer switching valve		
Maximum flow area, A_{max}	0.0012	m^3
Transition ratio	0.05	
Switching frequency	20	Hz

TABLE 4. PHYSICAL PARAMETERS

Working fluid: seawater at 25 ℃ with 35000 ppm NaCl		
Density, ρ	1023	$kg\ m^{-3}$
Absolute viscosity, μ	$9.4x10^{-4}$	Pa s
Bulk modulus, β	2.2	GPa
Entrained air volume fraction at atmospheric pressure, R	0.005	
Accumulator charge gas: air		
Specific heat, γ	1.4	

TABLE 5. PIPING PARAMETERS

Intermediate line		
Length	10	m
Inner diameter	0.1	m
High-pressure pipeline		
Length	500	m
Inner diameter	0.1	m
Sonic velocity	1460	$m\ s^{-1}$
Low-pressure pipeline		
Length	500	m
Inner diameter	0.1	m
Sonic velocity	920	$m\ s^{-1}$
Seawater intake pipeline, first reach		
Length	10	m
Inner diameter	0.1	m
Seawater intake pipeline, second reach		
Length	490	m
Inner diameter	0.1	m

TABLE 6. ACCUMULATOR PARAMETERS

	Volume (L)	Pre-charge (MPa)
RO inlet HPA	200	4
onshore HPA	100	20
offshore HPA	150	20
offshore LPA	150	0.1

TABLE 7. SWITCH-MODE TRANSFORMER PARAMETERS

Pump/motor displacement	450	$cm^3 rev^{-1}$
Generator moment of inertia	0.4	$kg\ m^2$
Switched volume, V_{sw}	500	cm^3
Switching frequency, f_{sw}	20	Hz

TABLE 8. ASSUMED COMPONENT EFFICENCIES

WEC-driven actuator mechanical, $\eta_{WEC,m}$	0.9
Pump/motor mechanical, $\eta_{pm,m}$	0.9
Pump/motor volumetric, $\eta_{pm,v}$	0.9
Generator, η_{gen}	0.9
Charge pump, η_{cp}	0.9

SIMULATION RESULTS

Two separate simulations were performed and are presented below. First is an isolated model of the switch-mode transformer with a constant pressure of 30 MPa as the controller set point pressure $p_{H,out}$, 6.9 MPa as the controller set point $p_{RO,ref}$, and a duty ratio of 0.6. Second, is the full model with 30 MPa as $p_{H,out,ref}$ and 6.9 MPa as $p_{RO,ref}$, a mean absolute actuator velocity, $|\dot{x}|_{ave}$, of 0.16 m s^{-1}, and a wave period, T_w, of 12 seconds.

Methods

These simulations were run until cyclical steady-state was reached. The model was solved numerically using an Euler solver with a time step of $5x10^{-6}$ seconds; however, the distributed parameter line models were solved at a larger time step of $1x10^{-3}$ seconds. The control inputs were updated with a time step of 0.01 seconds.

Results

The dynamics of the switch-mode transformer from the isolated switch-mode transformer simulation are presented in Figure 5. Two switching cycles are shown. Subplot A presents the pressure in the switched volume and the area fraction of the switching valve, while subplot B presents the flow rates in and out of the volume.

Two features of the dynamics are evident. First, there is a significant spike in flow rate as the switching valve opens coupled with a high pressure drop across the valve. Second is the positive and negative ramps in flow rate during the two discrete parts of the switching cycle created by the acceleration and deceleration of the pump/motor and generator shaft speed.

The results of the full system simulation are now presented for one steady-state wave cycle (12 seconds).

First, the behavior of the controlled states and control inputs are given in Figure 6. The control of the RO inlet pressure is shown in the top plot. The RO pressure varies at two different time scales. At the time scale of the PWM switching, the pressure varies with a relatively low magnitude, but with high rates of change due to the high switching frequency; this is most obvious just after 4 seconds where the line appears to thicken due to a high rate oscillation. The filtered signal lags a little but has a substantially reduced magnitude of variation. At the longer time scale, the pressure varies with the dynamics of the long pipeline; although, the pressure variation is less than 0.1 MPa. The torque demand from the generator varies considerably as well. At the longer time scale, the torque varies with an amplitude of nearly 400 Nm. At the time scale of switching however, there is only a small apparent variation.

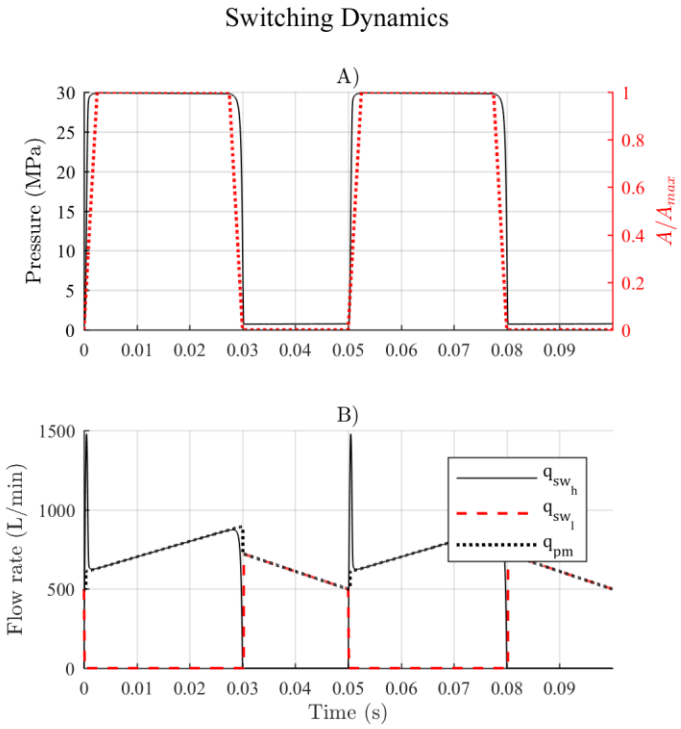

FIGURE 5. SWITCH-MODE TRANSFORMER DYNAMICS.

In the second subplot of Figure 6, the WEC load control is shown to maintain the pressure of the onshore HPA near the reference pressure with variation having an amplitude of about 2 MPa. The duty varies about a mean of about 0.5 and with an amplitude of 0.2.

In Figure 7, the pressure and flow dynamics of the WEC-driven pumping are shown. The same pressure traces are shown at different scales in subplots A and B for visualization of the chamber pressure behavior during both direction reversals of the WEC. The accumulator pressures are given as well, and show the pressure drop across the check valve rectifier. Subplot C shows the flow rate in and out of the WEC-driven actuator. An important feature of these dynamics is the interruption of flow when the WEC reverses direction (at 0 seconds and 6 seconds). During this period of interruption, there is compression and decompression of the individual pumping chambers until the pressure differences across the check valves reach the cracking pressure. Through part of this compression/decompression, power will be flowing from the actuator through the WEC and to the surroundings and could be considered a loss.

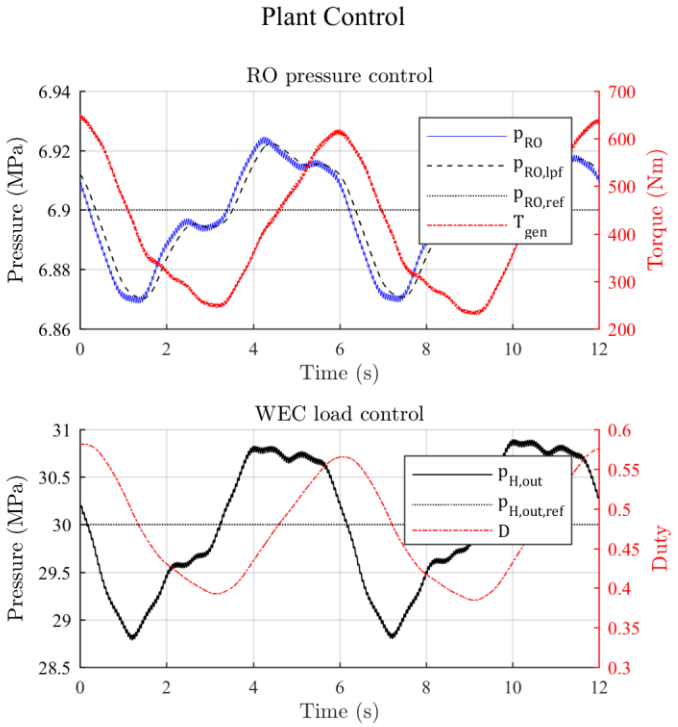

FIGURE 6. PLANT CONTROL BEHAVOIR IN CYCLIC STEADY-STATE.

The dynamics of the high and low-pressure pipelines are given in Figure 8 and Figure 9, respectively. Each of these show significant pressure wave delay effects. Subplot A of Figure 8 reveals that the difference between the inlet and outlet pressure of the high-pressure pipeline switches direction with a period of about 1 second, while the WEC oscillates with a period of 12 seconds. In subplot B, a difference and delay in flow rates in and out reveal the storage and release of energy in the pipeline. Some smoothing of flow by the pipeline is evident with the lower magnitude of the out flow.

The behavior of the low-pressure pipeline appears different in nature, likely owing to the constant pressure boundary condition upstream. These dynamics are significant nonetheless. In subplot A of Figure 9, the pressure varies with an amplitude of about 1 MPA about a mean of 1 MPA. In subplot B, the flow rate is about

90 degrees out of phase with the flow rate through the check valve rectifier. At 2 and 8 seconds, the flow rate out of the pipe drops near zero. The storage and release of fluid is apparent with the difference in flow in and out of the pipe, as with the high-pressure line.

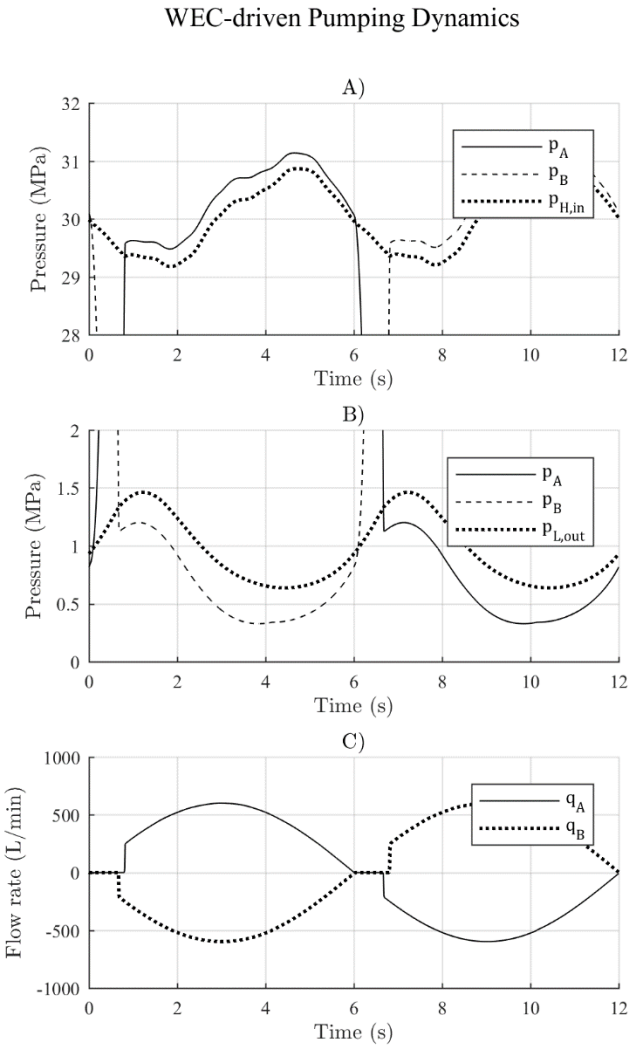

FIGURE 7. WEC-DRIVEN PUMPING DYNAMICS.

Quantified Results

To quantify the performance of the plant the following efficiencies are defined.

The efficiency of the pumping system composed of the WEC-driven actuator and the check valve rectifier is defined by

$$\eta_{WEC\ pump} = \frac{\int \left((q_{c3} + q_{c4}) p_{H,in} - (q_{c1} + q_{c2}) p_{L,out} \right) dt}{\int \max(F\dot{x}, 0)\, dt} \qquad (35).$$

Note that a negative result of $F\dot{x}$ corresponds to the WEC doing work on the surroundings and is considered a power loss. This is removed by the $\max(*)$ operator.

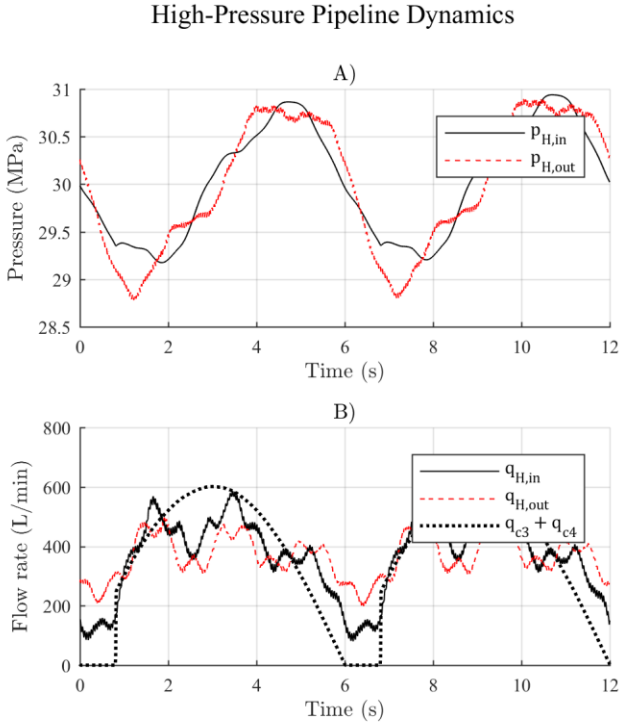

FIGURE 8. HIGH-PRESSURE PIPELINE DYNAMICS.

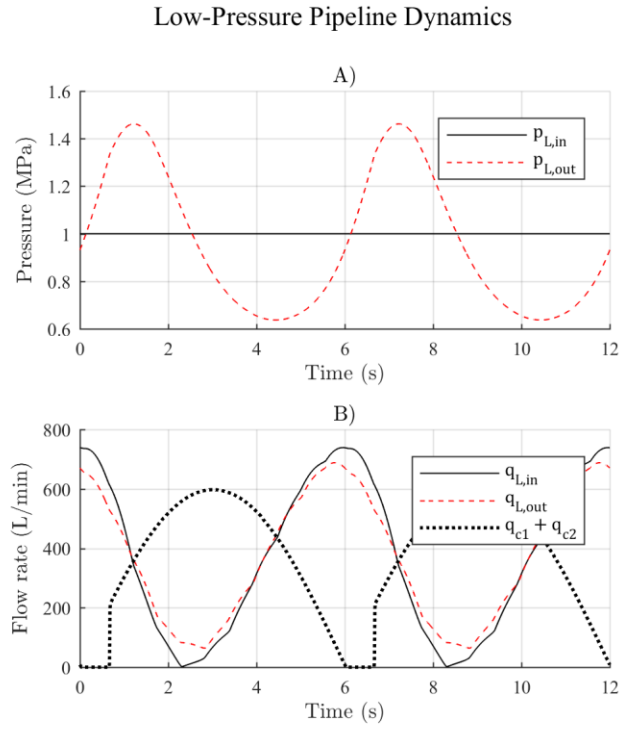

FIGURE 9. LOW-PRESSURE PIPELINE DYNAMICS.

The efficiency of power transformer is defined as

$$\eta_{pt} = \frac{\int \left(q_{pm}\left(p_{RO} - p_{L,in}\right) + T_{pm}\omega\right) dt}{\int q_{sw,h}\left(p_{H,out} - p_{L,in}\right) dt} \qquad (36)$$

with the work delivered to the RO system and to the generator at the shaft as outputs and the work from the high-pressure line as the input.

The efficiency of the entire system – taking the work done by the WEC on the actuator as the input and taking the surplus electrical energy production and hydraulic work delivered to the RO system as outputs – is expressed as

$$\eta_{sys} = \frac{\int \left(q_{RO}(p_{RO} + p_o) + q_{ERU,in}(p_{L,in} + p_o) + P_{gen,elec} - P_{cp}\right) dt}{\int \max(F\dot{x}, 0)\, dt} \qquad (37).$$

Note that this neglects the electrical power required to operate the energy recovery device or any other power consuming device in the RO system.

The efficiency results, mean power captured, mean electrical power produced, mean power consumed by the charge pump, and the mean surplus power (the produced electrical power minus the power consumed by the charge pump) are given in Table 9. The losses in the system are tabularized in the order of descending magnitude in Table 10.

Discussion

It is evident that the switch-mode transformer accomplishes the goal to decouple the pressures of the power take-off and RO process. Additionally, the efficiency for the power transformer at 76% suggests that this is a better approach than the conventional power transformer, which would likely be in the range of 65-70% – assuming a total efficiency of 0.81 for both the pump and motor).

TABLE 9. POWER AND EFFICENCY RESULTS

WEC power capture	205	kW
electrical power generated, mean	56.9	kW
electrical power consumed by charge pump, mean	53.7	kW
surplus electrical power generated, mean	3.22	kW
actuator pumping efficiency, $\eta_{WEC\ pump}$	0.864	
switch-mode power transformer efficiency, η_{pt}	0.764	
system efficiency, η_{sys}	0.450	

More generally, the primary losses are found to be from the pump/motor, charge pump, WEC mechanical operation, and generator; naturally, each of these are major functional components. The losses from the valves for the switch-mode power transformer total 8.3 kW, which accounts for 4% of the losses in the entire circuit; this is a small cost in power in the way of enabling the decoupling of the pressures of the wave energy harvesting process and RO process. The piping losses not associated with the intake total less than 1 kW; these are clearly oversized. The unsteady piping losses are very low and are likely to be negligible, even for more optimally sized pipelines.

TABLE 10. MEAN POWER LOSS RESULTS

Pump/motor	33.6	kW
Charge pump	24.7	kW
WEC mechanical loss	20.5	kW
Generator	10.0	kW
Intake piping	8.11	kW
Switching valve	6.78	kW
Check valve rectifier	3.95	kW
Switch-mode check valve	1.46	kW
Low-pressure pipeline, steady	0.367	kW
High-pressure pipeline, steady	0.207	kW
Low-pressure pipeline, unsteady	0.0270	kW
Intermediate line	0.0120	kW
High-pressure pipeline, unsteady	0.00757	kW

It is also evident that the dynamics of a wave-powered plant are extreme and may pose a challenge to the designer, especially the pipeline dynamics. Although, the pipeline dynamics may be significantly damped by selecting a smaller diameter pipeline. This study assumed simple, sinusoidal WEC motions, when in fact realistic waves are very irregular. In these irregular waves the WECs have much greater peak-to-mean power capture. This would only further complicate the dynamics and produce more extreme transient behavior. Good control of the plant was obtained in this study but the control performance with more realistic WEC motions would be interesting.

Apart from the system dynamic aspects plant, which have been the focus of this study, a number of remaining challenges should be pointed out. First, seawater compatible fluid power components are not widely available outside of the reverse osmosis application; although axial piston pumps are available from the manufacturer Danfoss [21] whose design might be modified for use as motors. Second, fast switching valves still need to be developed; however, the scale of the system herein lends itself to lower switching frequencies which might make this system more amenable to realization than other, smaller switch-mode systems.

CONCLUSION

This study has demonstrated a unique application of a switch-mode hydraulic system. In fact, it solves an inherent problem in implementing a wave-powered RO desalination plant. The study also reveals the complex and extreme behaviors that should be expected with a long pipeline in any wave energy plant having a hydraulic power take-off.

ACKNOWLEDGEMENT

The authors acknowledge the support of Resolute Marine Energy, Inc. through a subcontract of the Department of Energy SBIR Phase II Grant No. DE-SC0017699.

REFERENCES

[1] R. Henderson, "Design, simulation, and testing of a novel hydraulic power take-off system for the Pelamis wave energy converter," in *Renewable Energy*, 2006, vol. 31, no. 2, pp. 271–283.

[2] L. O'Boyle, K. Doherty, J. van 't Hoff, and J. Skelton, "The Value of Full Scale Prototype Data - Testing Oyster 800 at EMEC , Orkney," *Proc. 11th Eur. Wave Tidal Energy Conf.*, no. November, pp. 1–10, 2015.

[3] M. Penalba and J. V. Ringwood, "A review of wave-to-wire models for wave energy converters," *Energies*, vol. 9, no. 7, 2016.

[4] C. J. Cargo, A. Hillis, and A. R. Plummer, "Optimisation and control of a hydraulic power take-off unit for a wave energy converter in irregular waves," *Proc. Inst. Mech. Eng. Part A J. Power Energy*, vol. 228, no. 4, pp. 462–479, 2014.

[5] R. H. Hansen, M. M. Kramer, and E. Vidal, "Discrete displacement hydraulic power take-off system for the wavestar wave energy converter," *Energies*, vol. 6, no. 8, pp. 4001–4044, 2013.

[6] A. R. Plummer and M. Schlotter, "Investigating the Performance of a Hydraulic Power Take-Off," *Proc. Eighth Eur. Wave Tidal Energy Conf.*, pp. 729–735, 2009.

[7] D. Dießel, G. Bryans, L. Verdegem, and H. Murrenhoff, "Wavepod a transmission for wave energy converters - set-up and testing," *Int. J. Fluid Power*, vol. 16, no. 2, pp. 75–82, 2015.

[8] "Resolute Marine Energy." [Online]. Available: http://www.resolutemarine.com/. [Accessed: 15-Apr-2019].

[9] M. Folley, B. Suarez, and T. Whittaker, "An autonomous wave-powered desalination system," *Desalination*, vol. 220, pp. 412–421, 2008.

[10] P. A. Davies, "Wave-powered desalination: Resource assessment and review of technology," *Desalination*, vol. 186, no. 1–3, pp. 97–109, 2005.

[11] D. C. Hicks, C. M. Please, G. R. Mitcheson, and J. F. Salevan, "Delbuoy: Ocean Wave-Powered Seawater Reverse Osmosis Deslination System," *Desalination*, vol. 73, pp. 81–94, 1989.

[12] Y. Yu, "Numerical Modeling and Dynamic Analysis of a Wave-Powered Reverse-Osmosis System," 2018.

[13] C. Yuan, M. Pan, and A. Plummer, "A Review of Switched Inertance Hydraulic Converter Technology," in *BATH/ASME 2018 Symposium on Fluid Power and Motion Control*, 2018.

[14] F. Wang, L. Gu, and Y. Chen, "A continuously variable hydraulic pressure converter based on high-speed on–off valves," *Mechatronics*, vol. 21, pp. 1298–1308, 2011.

[15] B. Cho, H. Lee, and J. Oh, "Estimation Technique of Air Content in Automatic Transmission Fluid by Measuring Effective Bulk Modulus," *Int. J. Automot. Technol.*, vol. 3, no. 2, pp. 57–61, 2002.

[16] E. B. Wylie, V. L. Streeter, and L. Suo, *Fluid Transients in Systems*. Upper Saddle River, NJ: Prentice Hall, 1993.

[17] A. Trikha, "An Efficient Method for Simulating Frequency-," *J. Basic Eng.*, vol. March, pp. 97–105, 1975.

[18] G. A. Schohl, "Improved Approximate Method for Simulating Frequency-Dependent Friction in Transient Laminar Flow," *J. Fluids Eng.*, vol. 115, no. 3, p. 420, 2008.

[19] A. C. Yudell and J. D. Van de Ven, "Experimental Validation of a Time Domain Cavitation Model for Switched Inertance Circuits," in *Proceedings of the ASME/BATH Symposium on Fluid Power and Motion Control*, 2017.

[20] I. Rühlicke and M. Haag, "Oyster Wave Energy Power Plant: A New Challenge for Hydraulic Cylinders," *Hydraulics & Pneumatics*, 2013.

[21] "Danfoss." [Online]. Available: https://www.danfoss.com/en-us. [Accessed: 15-Apr-2019].